Voltage-tunable dual-band quantum dot infrared photodetectors for temperature sensing

Hong-Shi Ling,[1] Shiang-Yu Wang,[1,*] Wei-Cheng Hsu,[2] and Chien-Ping Lee[2]

[1]*Institute of Astronomy and Astrophysics, Academia Sinica, P.O. Box 23-141, Taipei, Taiwan*
[2]*Department of Electronic Engineering, National Chiao Tung University, 1001 Ta Hsueh Road, Hsinchu 300, Taiwan*
**sywang@asiaa.sinica.edu.tw*

Abstract: We report voltage-tunable 3-5 μm & 8-12 μm dual-band detection in the $InAs/Al_{0.3}Ga_{0.7}As/In_{0.15}Ga_{0.85}As$ confinement-enhanced dots-in-a-well quantum dot infrared photodetectors. The capability in temperature sensing is also demonstrated. Distinct response peaks at 5.0 μm and 8.6 μm were observed in the photocurrent spectra with working temperature up to 140K. The two peaks correspond to the transition paths from the quantum dot ground state to the quantum well state and the quantum dot excited state, respectively. At 77K, the response ratio of the 8.6 μm peak over the 5.0 μm peak changes from 0.29 at –3V to 5.8 at + 4.8V. Excellent selectivity between the two peaks with bias voltage makes the device attractive for third-generation imaging systems with pixel-level multicolor functionality.

©2012 Optical Society of America

OCIS codes: (040.0040) Detectors; (040.5570) Quantum detectors.

References and links

1. A. Rogalski, J. Antoszewski, and L. Faraone, "Third-generation infrared photodetector arrays," J. Appl. Phys. **105**(9), 091101 (2009).
2. A. Majumdar, K. K. Choi, J. L. Reno, L. P. Rokhinson, and D. C. Tsui, "Electron transfer based voltage tunable two-color quantum well infrared photodetectors," Infrared Phys. Technol. **44**(5-6), 337–346 (2003).
3. B. F. Levine, "Quantum well infrared photodetectors," J. Appl. Phys. **74**(8), R1–R81 (1993).
4. Y. Arslan, S. U. Eker, M. Kaldirim, and C. Besikci, "Large format voltage tunable dual-band QWIP FPAs," Infrared Phys. Technol. **52**(6), 399–402 (2009).
5. P. Martyniuk, S. Krishna, and A. Rogalski, "Assessment of quantum dot infrared photodetectors for high temperature operation," J. Appl. Phys. **104**(3), 034314 (2008).
6. Z. Chen, E. T. Kim, and A. Madhukar, "Normal-incidence voltage- tunable middle- and long-wavelength infrared photoresponse in self-assembled InAs quantum dots," Appl. Phys. Lett. **80**(14), 2490–2492 (2002).
7. M. J. Meisner, J. Vaillancourt, and X. Lu, "Voltage-tunable dual-band InAs quantum-dot infrared photodetectors based on InAs quantum dots with different capping layers," Semicond. Sci. Technol. **23**(9), 095016 (2008).
8. G. Ariyawansa, A. G. U. Perera, G. Huang, and P. Bhattacharya, "Wavelength agile superlattice quantum dot infrared photodetector," Appl. Phys. Lett. **94**(13), 131109 (2009).
9. J. Huang, W. Ma, Y. Wei, Y. Zhang, Y. Huo, K. Cui, and L. Chen, "Two-color $In_{0.4}Ga_{0.6}As/Al_{0.1}Ga_{0.9}As$ quantum dot infrared photodetector with double tunneling barriers," Appl. Phys. Lett. **98**(10), 103501 (2011).
10. H. S. Ling, S. Y. Wang, and C. P. Lee, "Spectral response and device performance tuning of long-wavelength InAs QDIPs," Infrared Phys. Technol. **54**(3), 233–236 (2011).
11. S. Krishna, D. Forman, S. Annamalai, P. Dowd, P. Varangis, T. Tumolillo, A. Gray, J. Zilko, K. Sun, M. Liu, J. Campbell, and D. Carothers, "Demonstration of a 320×256 two-color focal plane array using InAs/InGaAs quantum dots in well detectors," Appl. Phys. Lett. **86**(19), 193501 (2005).
12. J. Vaillancourt, P. Vasinajindakaw, X. Lu, A. Stintz, J. Bundas, R. Cook, D. Burrows, K. Patnaude, R. Dennis, A. Reisinger, and M. Sundaram, "A voltage-tunable multispectral 320 × 256 InAs/GaAs quantum-dot infrared focal plane array," Semicond. Sci. Technol. **24**(4), 045008 (2009).
13. J. Andrews, W. Y. Jang, J. E. Pezoa, Y. D. Sharma, S. J. Lee, S. K. Noh, M. M. Hayat, S. Restaino, S. W. Teare, and S. Krishna, "Demonstration of a bias tunable quantum dots-in-a-well focal plane array," Infrared Phys. Technol. **52**(6), 380–384 (2009).
14. H. S. Ling, S. Y. Wang, C. P. Lee, and M. C. Lo, "High quantum efficiency dots-in-a-well quantum dot infrared photodetectors with AlGaAs confinement enhancing layer," Appl. Phys. Lett. **92**(19), 193506 (2008).
15. H.-S. Ling, S.-Y. Wang, C.-P. Lee, and M.-C. Lo, "Long-wavelength quantum-dot infrared photodetectors with operating temperature over 200K," IEEE Photon. Technol. Lett. **21**(2), 118–120 (2009).
16. S. Y. Wang, S. D. Lin, H. W. Wu, and C. P. Lee, "High performance InAs/GaAs quantum dot infrared photodetectors with AlGaAs current blocking layer," Infrared Phys. Technol. **42**(3-5), 473–477 (2001).

#162350 - $15.00 USD Received 1 Feb 2012; revised 20 Feb 2012; accepted 7 Mar 2012; published 20 Apr 2012
(C) 2012 OSA

1. Introduction

Dual/multiple band infrared (IR) detectors are essential for advanced IR imaging systems because of the capability of not only detection but also discrimination and identification for targets [1]. For example, a dual-band focal plane array (FPA) camera enables remote temperature sensing of grey bodies with unknown but constant emissivity. Single FPAs with dual-band detection eliminate the heavy and complex optical components required in the systems based on two separate single band FPAs or a broad-band FPA system with filters, leading to smaller and simpler instrument. By stacking two different absorption layers, dual-bands FPAs with different material systems have been demonstrated [1]. In general, the stacking structure requires more contacts and indium bump for the array fabrication, unless voltage tuning structures are designed. The capability to tailor the spectral response of the device by voltage is especially desirable since it allows dual-band FPAs with single indium bump for each pixel, which greatly simplifies the fabrication process and increases the yield.

In the past, voltage tuning of response spectrum has been demonstrated with quantum well infrared photodetectors (QWIPs) [2,3]. However, due to the structure limitations, only the voltage tuning stacking structure QWIPs can offer good performance at 77K with large tunable wavelength region. 640 × 512 QWIP FPA with voltage-tunable stacking structure has been demonstrated [4]. With the same benefit from mature GaAs based technology as QWIPs, quantum dot infrared photodetectors (QDIPs) are developed with more sophisticated device structures and make it possible to collect photoelectrons from different transition paths and thereby achieve dual-band detection. Besides, with three dimensional confinement structure and suppressed electron-phonon interactions, QDIPs are predicted to be able to absorb normal incident light and provide high temperature operation [5]. With these motivations, QDIPs have been widely studied in the past decade and the voltage-tunable dual-band operations using different designs have been demonstrated by many groups [6–13]. Some results are also implemented into FPAs [11–13]. However, the previous reports did not present a very desirable spectral feature that comprises narrow peaks located separately at mid-wave IR (MWIR, 3-5 μm) and long-wave IR (LWIR, 8-12 μm) atmospheric windows and also shows low spectral cross-talk on the two-color operation. In this paper, we report the voltage-tunable dual-band operation of QDIPs with narrow response peaks at 5 μm & 8.6 μm and good selectivity between the two peaks. The device application for temperature sensing is also examined.

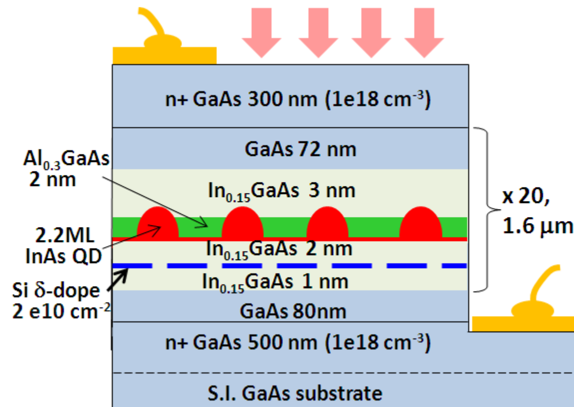

Fig. 1. Schematic epitaxy structure of the sample.

2. Sample growth and wafer characterization

The device sample was grown by a Varian GEN-II molecular beam epitaxy machine on (001) semi-insulating GaAs substrate. Figure 1 shows the schematics of the device structure. 20 period stacks of absorption structure separated by GaAs barrier layers were grown as the

#162350 - $15.00 USD Received 1 Feb 2012; revised 20 Feb 2012; accepted 7 Mar 2012; published 20 Apr 2012
(C) 2012 OSA

active region and sandwiched by two n + GaAs contact layers. Each QD layer consists of 3 nm bottom $In_{0.15}Ga_{0.85}As$ layer, 2.2 monolayers of InAs QDs, 2 nm $Al_{0.3}Ga_{0.7}As$ layer and 3 nm top $In_{0.15}Ga_{0.85}As$ layer. Besides, the uncapped QDs with 3 nm bottom $In_{0.15}Ga_{0.85}As$ and 2.2 monolayers of InAs layers were also deposited on the surface for AFM characterization of QDs. The inserted thin AlGaAs layer on the QD layer enhances the quantum confinement for the InAs QDs states embedded in the GaAs/InGaAs quantum well (QW). This structure, so called confinement-enhanced dots-in-a-well (CE-DWELL), was proven to effectively increase the quantum efficiency of device and also provide desirable LWIR detection [14,15]. Furthermore, the addition of AlGaAs layer provides more parameter in tuning the response wavelength and device performance [10]. In our previous studies, the LWIR response peak wavelength scatters from sample to sample in the range of 7-10 μm for CE-DWELL structure. The LWIR peak was attributed to the intersubband transition between QD ground state to QD excited state (hereafter Ψ_o-to-Ψ_n) from the photoluminescence (PL) and PL excitation (PLE) spectrum. Meanwhile, the transition from the QD ground state to the QW state (hereafter Ψ_o-to-Ψ_{2D}) was also observed in some of the samples. The Ψ_o-to-Ψ_{2D} absorption could be enhanced by increasing the InGaAs well width in the CE-DWELL structure [10]. However, such Ψ_o-to-Ψ_{2D} response wavelength revealed was not short enough to fit the mid infrared atmospheric window (around 6 μm). Based on the aforementioned result, we fine-tuned the growth parameters for InAs QDs and InGaAs QW to manipulate the transition energies of Ψ_o-to-Ψ_n and Ψ_o-to-Ψ_{2D} to achieve desirable LWIR & MWIR dual-band detection. More specifically, we managed to shift the Ψ_o-to-Ψ_{2D} response into the MWIR band while maintaining the Ψ_o-to-Ψ_n response peak longer than 8 μm for the current sample.

In addition to the transition wavelength, the oscillator strength and the escape probability of photoelectrons for the 2D state transition is also important to generate reasonable photocurrent at right wavelength [10]. However, these parameters also vary with the device structure. Considering both the responsivity strength and transition wavelength, we have investigated extensively to optimize QW thickness combination of the InGaAs layers above and beneath the QDs. Moreover, QDs with large sizes were deliberately grown (with higher growth temperature) to enlarge the energy difference between the QD ground state and the 2D state. The PL and PLE spectroscopy were used to probe the electronic state energy of the sample at 77K as shown in Fig. 2. Sharp peak of the 2D state is observed implying clear wavefunction confinement of the state. From Fig. 2, the transition energy for the ground state and the 2D state are 1.007 eV and 1.445 eV, respectively. The energy separation of 438 meV assuming 60% on conduction band corresponds to 4.72 μm, indicating that the intersubband transition of Ψ_o-to-Ψ_{2D} absorbs infrared radiation in the MWIR window. The Ψ_o-to-Ψ_{2D} transition was successfully manipulated to generate strong MWIR response. A small shoulder peak at around 1.13 eV was also observed in the PL spectrum. Owing to the low power excitation (~1 W/cm^2), such a shoulder peak at high energy side refers to presence of the QDs with smaller sizes and minor population in the sample beside the main QD group instead of signal of excited state. Such small-size dots were also confirmed by the AFM image inset in Fig. 2.

#162350 - $15.00 USD Received 1 Feb 2012; revised 20 Feb 2012; accepted 7 Mar 2012; published 20 Apr 2012
(C) 2012 OSA

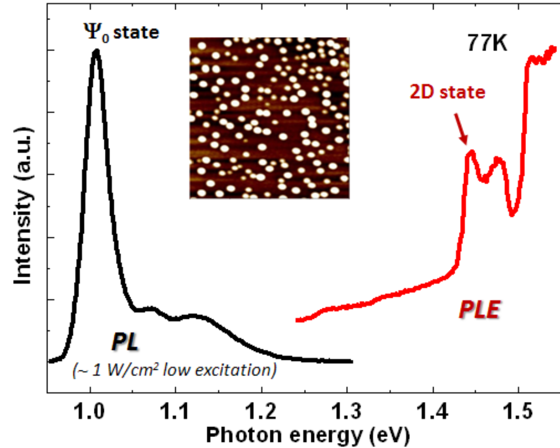

Fig. 2. PL and PLE spectra of the sample at 77K. The inset shows the 1 μm^2 AFM image of the sample.

3. Device fabrication and performance characterization

Standard processing techniques were then applied for the device fabrication. 260 × 370 μm^2 mesas with AuGe contact rings were formed to allow normal incidence measurement from the mesa top. In all measurements, the bottom contact is referred as ground. The optical window size is about 200 × 200 μm^2. The photocurrent spectra were measured by a Fourier transform infrared spectrometer and the absolute responsivity was calibrated with 1000 °C blackbody radiation with a Ge wafer to filter out photons with wavelength shorter than 2 μm. The photocurrent spectrum of the sample at 140K and 3V is displayed in Fig. 3(a). Two well separated response signals at 5 μm & 8.6 μm were observed at such high working temperature. The operating temperature of 140K is so far the highest reported for the MWIR & LWIR dual-band QDIPs due the superior quantum efficiency of CE-DWELL structure. The responsivity of the two peaks is about 3 mA/W and the detectivity is about 4 × 10^6 Jones for both LWIR and MWIR peaks. With proper tuning of the CE-DWELL structure parameters, the Ψ_o-to-Ψ_{2D} transition peak is shifted toward MWIR band while the Ψ_o-to-Ψ_n transition peak is kept within LWIR band compared with our previous samples [10]. Excellent tunability of the two response peaks by voltage is also achieved. Figure 3(b) shows the response spectrum at two different biases at 77K. At −3V, the responsivity of 5 μm peak is much higher than that of the 8.6 μm peak due to higher escape probability of photoelectrons. On the other hand, when the bias voltage is changed to + 4.8V, the 8.6 μm peak dominates the response spectrum. Under positive bias, the excited state wavefunction shifts into the QD and the transition oscillator strength increases. With the strong electric field at 4.8V, the escape probability for excited photoelectron also increases. The responsivity ratio of the 8.6 μm peak over the 5 μm peak changes from 0.29 at −3V to 5.8 at + 4.8V. The voltage tunability, together with the narrow-width property from bound-to-bound transition (Δλ/λ is 8.4% for the 8.6 μm peak and is 15.8% for the 5 μm peak), leads to the two-color operations with low spectral cross-talk. The small signal in the 6-7 μm range observed in the 77K spectra while absent in the 140K spectrum is tentatively attributed to the Ψ_o-to-Ψ_{2D} transition of those small-size QDs mentioned previously in Fig. 2.

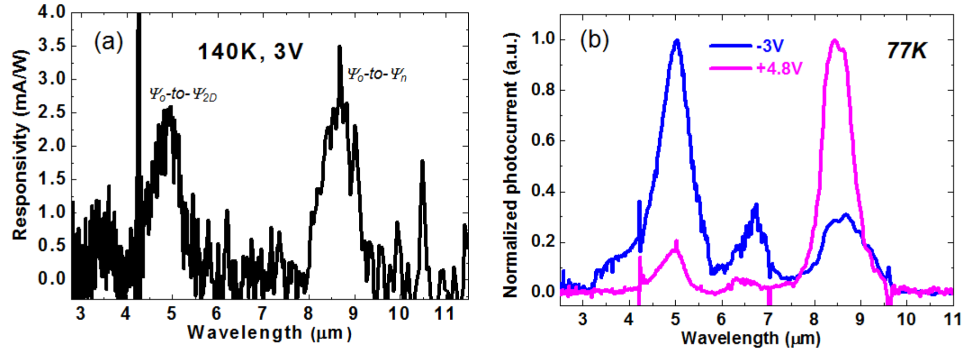

Fig. 3. Photocurrent spectra of the sample at (a) 140K and (b) 77K.

In addition to the bias polarity dependent response spectrum, low dark current with clear asymmetric behavior with bias polarity was also observed in the sample. At 77K, the dark current density is 8.4×10^{-7} A/cm^2 at + 3V and 1.5×10^{-5} A/cm^2 at −3V. Compared with the 10-period QDIPs with similar CE-DWELL structure we studied before, the dark current (under the same averaged electric field) of this 20-period device is about 109 times lower at forward bias and about 43 times lower at reverse bias. Even at a very high applied voltage of + 4.8V at 77K, the dark current density is only 5.8×10^{-5} A/cm^2 and the measured detectivity (for the LWIR peak) is still 1.9×10^9 Jones. The detectivity at lower biases should be much higher but it is not available due the limits of our noise measurement system. The noise current is lower than our system noise when the bias is between −3V to + 4.5V at 77K. The extremely low dark current at forward bias is partly due to the thin AlGaAs layer grown on InAs QDs [16] and also the more period stack in the active region. Low dark current is essential especially for the staring FPA applications.

4. Operation as a temperature sensor

With the parameters measured, the capability in temperature sensing of the device was examined. The photocurrent generated from the object is proportional to the responsivity and the incident infrared radiation. With a single pixel for dual-band operation, the incident infrared radiation only depends on the exitance from the object at different wavelength since the two bands share the same optics. The photocurrent ratio generated by the device at different bias polarities can be calculated by the following expression:

$$\frac{I_{ph+}}{I_{ph-}} = \frac{R_{p+}}{R_{p-}} \frac{\int \tilde{R}(\lambda,+4.8V)\,\varepsilon M(\lambda,T)\,d\lambda}{\int \tilde{R}(\lambda,-3.0V)\,\varepsilon M(\lambda,T)\,d\lambda}$$

where $\tilde{R}$ is the normalized spectral response at −3.0V and + 4.8V as shown in Fig. 3(b), M is the spectral exitance of blackbody radiation, ε is the emissivity of the sensing target, and R_p is the absolute peak resposivity, which is 268 mA/W at + 4.8V and 26.6 mA/W at −3V for the device at 77K. If the emissivity of the object is the same in the two detection bands, the expression suggests that the unknown emissivity of the target can be canceled out from the equation. The photocurrent ratio is then a function of only the target temperature and can be used to estimate the target temperature. The predicted photocurrent ratio of the sample we calculated for target temperature T from room temperature to 1000°C and plotted in Fig. 4. A clear non-linear dependency on T is obtained for the photocurrent ratio in this temperature range. The slope of the curve, irrespective of the negative sign, increases from 0.001 to 0.006 (#/°C) as the target temperature lowered from 1000 °C to 27°C. It is indicative that the sample, working as a temperature sensor, is much better for measuring room temperature objects than for high temperature objects. The weak dependency of photocurrent ratio on the high temperature region puts more rigorous precision requirement on the photocurrent

measurement. For sensing a room temperature target, given 5% error on the measurement of the device signal, then the error on the obtained target temperature can be 13 °C, but for a 1000°C target the error becomes 10 times severer, reaching 125 °C. We checked the validity of the sample as a temperature sensor with a blackbody from 1000 °C to 700 °C. The measured photocurrent ratio increase from 2.6 to 2.8. Comparing the measurement results to the calculated curve in Fig. 4, of which the photocurrent would increase from 2.6 to 2.9 with the temperature range, an increasing discrepancy toward lower temperature was found. Due to the limitation of system setup, our system was not able to generate reliable data when the blackbody temperature decreased. Smaller photocurrent from low temperature blackbody deteriorated the signal-to-noise ratio of the measurement system significantly and thereby made it difficult to obtain the true photocurrent ratio that was caused by the target. The large system noise prevented us to measure the photocurrent with lower blackbody temperature where the temperature sensing is more effective. However, in the real FPA application, the system noise can be effectively removed. The device should be able to show precise temperature measurement for objects near room temperature.

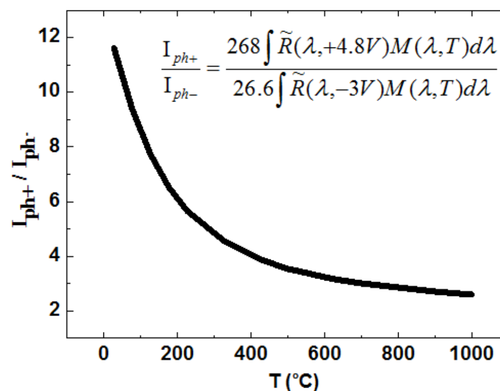

Fig. 4. The photocurrent ratio calculated for the sample at + 4.8V & −3V at 77K as a function of target temperature.

5. Summary

In summary, we report the voltage-tunable MWIR & LWIR dual-band operation in the CE-DWELL QDIPs. By manipulating the transition energies of InAs QDs and InGaAs QW in the CE-DWELL structure, distinct narrow response peaks at 5.0 µm & 8.6 µm in the photocurrent spectra were obtained for QDIPs up to 140K. Excellent selectivity between the two peaks by voltage change was obtained at 77K and the spectral results were used to demonstrate the application on temperature sensing. The device was shown to be more suitable for measuring room temperature objects than higher temperature objects. The results in this paper suggest that QDIPs with CE-DWELL structures are of great potential to be high-temperature operation multicolor detectors which are desirable for third-generation IR imaging systems.

Acknowledgments

This work was partly supported by the National Science Council of Taiwan under contract number NSC 98-2112-M-001-020-MY3.